Title

Algal p-coumaric acid induces oxidative stress and siderophore biosynthesis in the bacterial symbiont Phaeobacter inhibens.

Journal

Cell chemical biology, 29(4)

Authors

Wu, Yihan
Li, Anran
Gitai, Zemer
et al.

Publication Date

2022-04-21

DOI

10.1016/j.chembiol.2021.08.002

Peer reviewed

HHS Public Access

Author manuscript

Cell Chem Biol. Author manuscript; available in PMC 2022 April 24.

Published in final edited form as:

Cell Chem Biol. 2022 April 21; 29(4): 670–679.e5. doi:10.1016/j.chembiol.2021.08.002.

Algal *p*-coumaric acid induces oxidative stress and siderophore biosynthesis in the bacterial symbiont *Phaeobacter inhibens*

Rurun Wang[1,3], **Étienne Gallant**[1], **Maxwell Z. Wilson**[2,4], **Yihan Wu**[1,5], **Anran Li**[2], **Zemer Gitai**[2], **Mohammad R. Seyedsayamdost**[1,2,6,*]

[1]Department of Chemistry, Princeton University, Princeton, NJ 08544, USA

[2]Department of Molecular Biology, Princeton University, Princeton, NJ 08544, USA

[3]Present address: Exploratory Science Center, Merck & Co., Inc., Cambridge, MA 02141, USA

[4]Present address: Department of Molecular, Cellular, and Developmental Biology, University of California at Santa Barbara, Santa Barbara, CA 93106, USA

[5]Present address: Department of Environmental and Chemical Engineering, Shanghai University, Shanghai 200444, China

[6]Lead contact

SUMMARY

The marine alpha-proteobacterium *Phaeobacter inhibens* engages in intermittent symbioses with microalgae. The symbiosis is biphasic and concludes in a parasitic phase, during which the bacteria release algaecidal metabolites in response to algal *p*-coumaric acid (pCA). The cell-wide effects of pCA on *P. inhibens* remain unknown. Herein, we report a microarray-based transcriptomic study and find that genes related to the oxidative stress response and secondary metabolism are upregulated most, while those associated with energy production and motility are downregulated in the presence of pCA. Among genes upregulated is a previously unannotated biosynthetic gene cluster and, using a combination of gene deletions and metabolic profiling, we show that it gives rise to an unreported siderophore, roseobactin. The simultaneous production of algaecides and roseobactin in the parasitic phase allows the bacteria to take up any iron that is released from dying algal cells, thereby securing a limited micronutrient.

Graphical Abstract

*Correspondence: mrseyed@princeton.edu.

AUTHOR CONTRIBUTIONS

R.W., E.G., M.Z.W., and M.R.S. designed the study. R.W., M.Z.W., A.L., and M.R.S. designed the microarray, conducted transcriptomic studies, and/or analyzed the resulting data. All other experiments were conducted and analyzed by R.W., E.G., and M.R.S. R.W. and M.R.S. wrote the manuscript with input from all authors.

DECLARATION OF INTERESTS

The authors declare no competing interests.

SUPPLEMENTAL INFORMATION

Supplemental information can be found online at https://doi.org/10.1016/j.chembiol.2021.08.002.

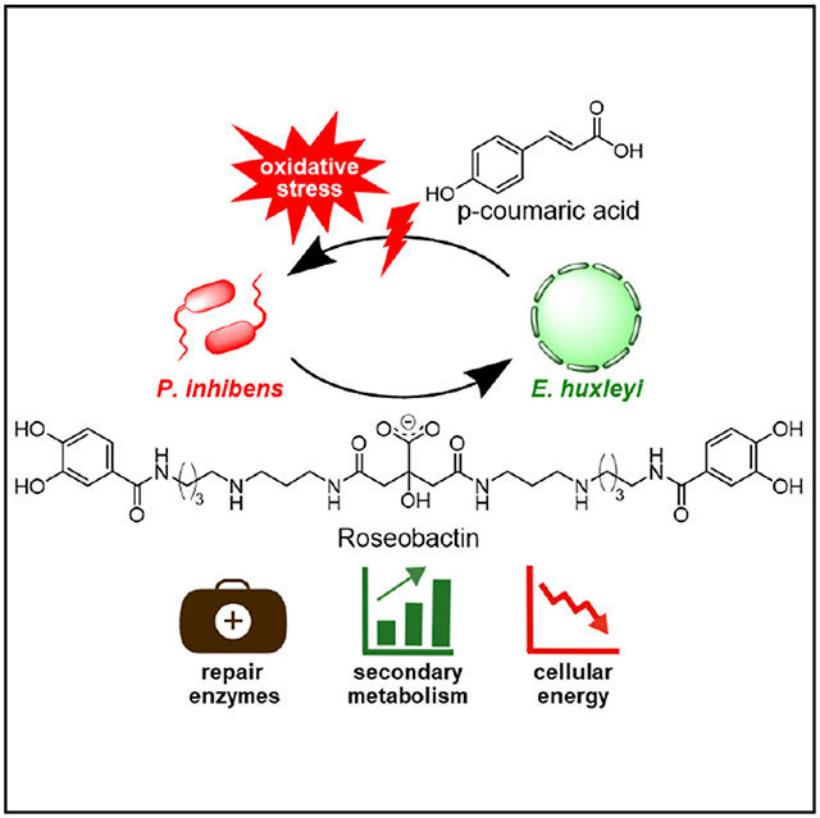

In brief

Microbial symbioses are mediated by the exchange of small molecule "words". Here, Wang et al. identify a new word in the algal-bacterial lexicon. They show that *p*-coumaric acid imparts oxidative stress and global transcriptional changes, leading to the synthesis of the siderophore, roseobactin.

INTRODUCTION

The *Roseobacter* form a physiologically distinct and metabolically diverse group of α-proteobacteria (Buchan et al., 2005; Wagner-Döbler and Biebl, 2006). They are especially abundant in coastal regions and participate in a number of important biogeochemical processes, such as global carbon and sulfur cycles, degradation of aliphatic and aromatic compounds, and intermittent interactions with eukaryotes (Brinkhoff et al., 2008; Geng and Belas, 2010). Anabolic pathways, that is, the capacity for secondary metabolite biosynthesis, facilitate microbial interactions, while catabolic pathways, which are encoded in many *Roseobacter*, enable their contribution to elemental cycles and utilization of organic matter. Because of these diverse roles, *Roseobacter* have recently received considerable attention in numerous ecology and laboratory-based studies. Understanding the molecular bases of these metabolic pathways provides insights into the disparate lifestyles of *Roseobacter* and carries important implications for the environment.

Our investigations into *Roseobacter* microbial interactions have focused on laboratory-based experiments with the model strain *Phaeobacter inhibens* and the primitive and widespread haptophyte *Emiliania huxleyi*. We have proposed a biphasic interaction model consisting of a mutualistically beneficial phase followed by a parasitic one (Seyedsayamdost et al., 2011a, 2011b) (Figure 1); a similar mutualist-to-parasite switch has subsequently been observed in other *Roseobacter*-phytoplankton associations as well (Wang et al., 2014, 2015; Mayers et al., 2016; Segev et al., 2016). The mutualistic phase is driven by the exchange of beneficial molecules: *E. huxleyi* and other microalgae produce and secrete sugars, amino acids, and dimethylsulfoniopropionate (DMSP), toward which *P. inhibens* and other marine bacteria chemotax (Seymour et al., 2010). *P. inhibens* can degrade DMSP and use it as a source of sulfur (González et al., 1999; Segev et al., 2016). In addition to nutrients, the microalgae also provide an attachment surface. About half a dozen *P. inhibens* cells can be seen to form direct contact with an *E. huxleyi* cell in laboratory co-culture, forming a microassembly that affords efficient exchange of small molecules (Segev et al., 2016). In response to the shelter and food provided by *E. huxleyi*, *P. inhibens* acts as a probiont and constitutively produces the potent antibiotic tropodithietic acid (TDA), which deters algal pathogens (Brinkhoff et al., 2004; Bruhn et al., 2005; Geng et al., 2008). Specifically, TDA dissipates the proton motive force, which is required for flagellar locomotion (Wilson et al., 2016). It has therefore been proposed that pathogens are hindered in their ability to access the TDA-producing microaggregate. *P. inhibens* also produces phenylacetic acid and indole-3-acetic acid, which serve as auxins and promote algal growth (Thiel et al., 2010; Segev et al., 2016). Several B vitamin biosynthetic pathways, such as thiamine, pyridoxamine, and cyanocobalamin, are encoded in *P. inhibens* as well; these may be a source of additional beneficial metabolites (Thole et al., 2012; Wagner-Döbler et al., 2010; Wienhausen et al., 2017).

The *P. inhibens*-microalgal interaction changes, however, when the algae secrete *p*-coumaric acid (pCA, Figure 1) or other phenylpropanoids, such as sinapic acid or ferulic acid (Martone et al., 2009; Espiñeira et al., 2011; Seyedsayamdost et al., 2011a, 2011b). Under these conditions, *P. inhibens* produces the roseobacticides, potent algaecides that kill *E. huxleyi*. A second algaecide, roseochelin B, is also elicited by sinapic acid. Roseochelin B is not as effective as the roseobacticides, but its production is widespread among *Roseobacter* strains and the compound is produced at higher titers (Wang and Seyedsayamdost, 2017). These algaecides are a hallmark of the parasitic phase of the interaction. The production of diverse secondary metabolites in nutrient-poor environments rests in part on the *Roseobacter*'s ability to divert the TDA biosynthetic pathway for roseobacticide production and to rely on spontaneous chemical transformations in roseochelin synthesis (Seyedsayamdost et al., 2014; Wang et al., 2016; Wang and Seyedsayamdost, 2017). The biosynthetic gene clusters for TDA, roseobacticide, and roseochelin were not predicted by bioinformatic explorations, as these are rather unusual secondary metabolites. Somewhat ironically, the products of a small number of gene clusters that can be located bioinformatically, including a 25-kb cluster that likely codes for a siderophore (Thole et al., 2012), have not yet been elucidated.

Several aspects of the mutualist-to-parasite or Jekyll-and-Hyde model remain to be examined. In the current study, we explore transcriptional changes in response to pCA

and the mechanism of elicitation of roseobacticides, focusing on *P. inhibens* 2.10, for which a completely assembled genome sequence was available at the inception of our work. *P. inhibens* 2.10 was isolated from the surface of the macroalga, *Ulva lactuca*, from a coast near Sydney in Australia (Thole et al., 2012; Dogs et al., 2013). It is highly related to the other *Phaeobacter* model, *P. inhibens* DSM 17395 (Thole et al., 2012). The two strains share 97% nucleotide similarity, a high level of conservation of genomic synteny, the ability to effectively colonize biotic and abiotic surfaces, as well as a similar capacity for synthesis of TDA, roseobacticides, and roseochelin B (Rao et al., 2006; Porsby et al., 2008; Seyedsayamdost et al., 2011b; Wang and Seyedsayamdost, 2017). We report the global transcriptomic response of *P. inhibens* 2.10 to pCA, which reveals cell-wide effects, notably energy depletion, sulfur assimilation, oxidative stress response, and secondary metabolism. Gene clusters coding for TDA and the elusive siderophore are significantly induced in response to pCA, a result that allowed us to isolate and structurally elucidate the product of this locus, an unreported catecholate siderophore, which we call roseobactin. The discovery of roseobactin adds an additional small molecule “word” to the bacterial-microalgal dialogue, and our transcriptomic studies provide further insights into the workings of the *P. inhibens*-microalgal symbiosis.

RESULTS

Global transcriptomic changes induced by pCA

The secondary metabolomic consequences of pCA treatment are well characterized (Seyedsayamdost et al., 2011a, 2011b). The global transcriptomic effects, however, are not, and we therefore initiated a microarray-based transcriptomic study of *P. inhibens* 2.10 (Tables S1 and S2), examining the effect of 1 mM pCA in early stationary phase cultures. Local concentrations of pCA are not known in co-cultures as the bacteria physically attach to an algal cell (Segev et al., 2016). One millimolar pCA has been used in previous studies and it effectively induces roseobacticide production (Seyedsayamdost et al., 2011a). Because roseobacticides accumulate in late stationary phase cultures, early stationary phase was chosen for monitoring transcriptomic changes. The addition of pCA has minimal effects on the growth curve of *P. inhibens* 2.10 (Figure S1).

Triplicate cultures were grown in the absence or presence of pCA, with total RNA isolated and subjected to DNA microarray analysis using an array that was devised *de novo* for *P. inhibens* 2.10 with three probes per open reading frame (see STAR Methods). Significant analysis of microarrays (SAM) showed that 1,171 genes (of 3,723 total) were differentially expressed with pCA (Data S1), accounting for nearly 31% of the genes encoded by *P. inhibens* 2.10 (Tusher et al., 2001). Among these, 604 genes were upregulated and 567 were downregulated compared with control (Figure S1). A histogram of differentially expressed genes revealed that 103 and 64 genes were upregulated and downregulated, respectively, 3-fold or more in response to pCA (Figure 2A, Data S1). The large number of differentially expressed genes indicates that pCA exerts cell-wide effects on transcription in *P. inhibens* 2.10. We analyzed the transcriptomic data using an untargeted approach, via the eggNOG mapper (Huerta-Cepas et al., 2017), and a targeted approach, via inspection of genes whose expression was altered most. EggNOG analysis provided an image of the effect of pCA

on the physiological pathways in *P. inhibens* 2.10 (Figure 2B). Among these, motility, energy production, secondary metabolism, and signal transduction (i.e., sensors and stress response elements) were the most affected by pCA. Visual inspection of the top up- and downregulated genes was largely in line with this conclusion (Table S3). We therefore set out to examine these pathways in more detail. Expression of motility and energy production genes were markedly downregulated, whereas those of secondary metabolism and stress responses/sensor domains were upregulated.

Effect of pCA on TDA biosynthesis

Two secondary metabolite loci were clearly upregulated by pCA in our transcriptomic data, the *tda* cluster and a putative siderophore gene cluster. Our previous studies with *P. inhibens* DSM17395 showed that large parts of TDA biosynthesis are borrowed to generate roseobacticides and that three different loci, the *tda* gene cluster, the *paa* catabolon, and the sulfur-metabolizing gene *patB*, are required for this process (Wang et al., 2016). Consistent with these results, pCA treatment led to a 3.7–13.5-fold induction of the *tda* gene cluster in *P. inhibens* 2.10; all operons within the cluster were positively regulated (Figures 3A and 3B, Table S4). The *paa* operon experienced a 1.7–4.4-fold induction with pCA, whereas the expression of *patB* did not change appreciably. A key component of TDA and roseobacticide biosynthesis is insertion of the thiol (TDA) or thiomethyl (roseobacticide A) groups, a process that requires sulfur assimilation. Accordingly, the *cysH*, *cysI*, and *fpr* genes inside of a putative sulfur assimilation operon were induced 7.4–15.2-fold.

To further verify that these loci are important for roseobacticide production in *P. inhibens* 2.10, we adapted the insertional mutagenesis protocol of *P. inhibens* DSM17395 and replaced four genes with a gentamicin resistance marker (*gnt*) to generate *tdaA::gnt* (*ΔtdaA*), *tdaD::gnt* (*ΔtdaD*), *paaC::gnt* (*ΔtdaC*), and *patB::gnt* (*ΔpatB*, Table S2) (Berger et al., 2011; Wang et al., 2016). All four mutants were viable and grew normally. They were, however, deficient in roseobacticide production when grown with pCA (Figure 3C), indicating that, like its relative, *P. inhibens* 2.10 also diverts the TDA pathway toward the production of roseobacticide, a rather unusual protocol for natural product biosynthesis (Wang et al., 2016). We note that TDA is synthesized constitutively by *P. inhibens* 2.10 in both phases of the symbiosis. The increased expression of *tda* in response to pCA does not significantly alter the yield of TDA (Figure S2). Instead, the now-stimulated pathway is diverted for roseobacticide biogenesis.

Effect of pCA on siderophore biosynthesis

Another secondary metabolite locus that was induced by pCA in our microarray data is a putative siderophore gene cluster previously identified by Brinkhoff and coworkers (Thole et al., 2012). We have named this cluster *rbt* (for roseobactin, see below); it was induced 3.3–6.7-fold in response to pCA (Figures 4A and 4B, Table S5). *Rbt* codes for non-ribosomal peptide synthetase-independent synthase (Challis 2005) and is homologous to the petrobactin cluster from *Bacillus anthracis* and *Bacillus cereus* (Barbeau et al., 2002; Abergel et al., 2008; Koppisch et al., 2008). Petrobactin is a unique siderophore that uses a bis-catechol substructure in combination with a citrate group to coordinate metals. In order to verify the microarray data, we first conducted RT-qPCR analysis with *rbtA* and *rbtE*, and

found them to be upregulated 8.7 ± 0.9-fold and 8.3 ± 0.4-fold, respectively, in response to pCA, in line with the microarray data. The production of a siderophore in response to pCA would have important implications for the algal-bacterial symbiosis, and we therefore set out to characterize the product of this cluster.

We generated a gene inactivation mutant, *rbtB::gnt* (*ΔrbtB*), and used the well-known chrome azurol S (CAS) assay to search for production of possible siderophores (Schwyn and Neilands, 1987). Under iron-depleted conditions, that is, nutrient-poor media supplemented with 100 μM EDTA, a CAS-positive fraction was detected in wild-type (WT) *P. inhibens* 2.10 treated with pCA, while the same fraction was negative in *ΔrbtB*. These two fractions were then subjected to untargeted high-resolution tandem mass spectrometry (HR-MS/MS) analysis. The WT contained a compound with m/z 719.3569, which matched the HR-MS of petrobactin (m/z 719.3616, ppm Δppm = 6.5) (Figure 4C). Under collision-induced dissociation, a fragment consistent with a catechol moiety (m/z observed, 137.0233; calculated, 137.0239; Δppm = 4.4) was detected. However, other fragments observed by HR-MS/MS were not consistent with petrobactin. The HR-MS/MS data suggest a similar molecular formula between roseobactin and petrobactin but different substructure compositions. The *ΔrbtB* mutant lacked both the parent ion and the catechol fragment (Figure 4C). These results together suggest that the putative petrobactin-like siderophore is the product of the *rbt* cluster.

To elucidate the structure of the new siderophore, large-scale production cultures were generated in the presence of EDTA and pCA. The siderophore was purified using a combination of open column and high-performance liquid chromatography (HPLC)-based separation methods, yielding ~3 mg of material from 4 L of culture. The siderophore was then subjected to 1D/2D NMR analysis. ^{1}H and correlated spectroscopy (COSY) data revealed four spin systems in a symmetrical molecule (Figure 4D, Table S6). One of these corresponds to a terminal 3,4-di-hydroxybenzoyl group. The others consist of a putrescine unit, propane-1,3-diamine, and citrate. The order of these substructures was determined from NMR and HR-MS/MS data to complete the structural elucidation of the siderophore. We have named this new siderophore roseobactin (Figure 4E). It differs from petrobactin in the order of the putrescine and propane-1,3-diamine units that connect the central citrate to the terminal catechol moieties (Figure 4F). A biosynthetic pathway can be proposed based on the petrobactin gene cluster and homology of the *rbt* genes (Lee et al., 2007; Hagan et al., 2018) (Figure S3). Consistent with this model, SAM decarboxylase, ornithine decarboxylase, and spermidine synthase, which provide the spermidine precursor for roseobactin, were upregulated 3.9–7.3-fold (Table S5). The elicitation of roseobactin by pCA suggests that the siderophore plays an important role in the parasitic phase of the symbiosis, likely allowing *P. inhibens* 2.10 to capture any iron released by the dying algal host in an environment where iron is limited. Moreover, the siderophore may aid in combating oxidative damage, as elaborated below.

pCA induces oxidative stress

Aside from TDA and roseobactin synthesis, inspection of upregulated genes also revealed many that are homologous to those involved in the oxidative stress response (Farr and

Kogoma, 1991; Storz and Imlay, 1999; Mishra and Imlay, 2012). Bacteria employ three strategies to cope with oxidative stress: (1) synthesis of metal chelators to sequester metals and prevent formation of free radicals or reactive oxygen species (ROS); (2) production of antioxidant enzymes, such as catalase, that deactivate ROS; and (3) activation of cell repair systems, including DNA repair, protein repair, and lipid repair to restore damaged biomolecules. All three categories of oxidative stress response are induced upon pCA exposure.

Representative of the first strategy is the induction of the *rbt* locus, which, as described above, is induced 3.3–6.7-fold upon pCA treatment and gives rise to roseobactin. Also upregulated is an interesting cluster of proteins coding for diverse siderophore transport proteins, with homology to the enterobactin-specific Fep proteins, hydroxamate-siderophore permeases, as well as a ferric-siderophore reductase for conversion of ferric to ferrous forms of iron (Figure S4). This locus was induced 2.2–5.9-fold in response to pCA, and it suggests that, although *P. inhibens* 2.10 does not code for the synthesis of tris-catecholate and hydroxamate siderophores, it has the ability to take up or "pirate" these from the environment under pCA-mediated stress. Additionally, heme biosynthesis and hemin uptake proteins were upregulated 7.5-fold and 3.6–5-fold, respectively. Heme can serve as an iron source for marine organisms (Roe et al., 2013; Hogle et al., 2014). It is also an important cofactor for antioxidant enzymes, which play roles in the second layer of oxidative response.

Representatives of the second category are at least five antioxidant and stress response enzymes, which show a significant 4.3–13.7-fold upregulation in the presence of pCA (Table S5). These include UspA, a universal stress response protein implicated in resistance to a variety of stationary phase stressors, including oxidative stress (Kvint et al., 2004; Nachin et al., 2005); OmpW, an adaptive stress response outer membrane protein (Xiao et al., 2016); KatG, a catalase-peroxidase with an established role in consuming ROS; cytochrome *c* peroxidase, which converts H_2O_2 to water using heme; and finally 1-Cys peroxiredoxin, which also reduces H_2O_2 to water (Zhang et al., 1992; Chen et al., 2000; Mishra and Imlay, 2012). The last three enzymes are typically induced in response to oxidative stress and involved in removing ROS.

Lastly, the transcriptomic results showed that repair systems were induced in response to pCA (3.3–14.9-fold, Table S5). These include *recA* and *mutT*, involved in DNA repair, as well as GMP synthetase (*guaA*) and the iron-free, vitamin B_{12}-dependent ribonucleotide reductase (*nrdJ*), which contribute to *de novo* DNA synthesis (Taddei et al., 1997; Stubbe, 2000; Schlacher and Goodman, 2007). Cell wall synthesis and ribosome biogenesis were induced as well. GlmU, which catalyzes an early committed step in cell wall synthesis, and GlmS, which generates hexosamines required for peptidoglycan production, were induced 5-fold. Moreover, the expression of 15 different ribosomal protein-coding genes (*rpsL*, *rpsG*, *rplB*, *rplD*, *rplT*, *rpmI*, *rplS*, *rplJ*, *rpsT*, *rplW*, *rpsD*, *rpmJ*, *rplV*, *rplR*, and *rpsK*) was positively regulated 2.7–4-fold, and all ribosomal proteins were induced 1.5–4-fold. The increased expression of these three categories of genes is consistent with pCA imparting oxidative stress onto *P. inhibens* 2.10. Although pCA is generally considered to be an antioxidant in plants, it has growth-inhibitory activity against several bacterial genera (Korkina, 2007; Lou et al., 2012). It does not significantly inhibit *P. inhibens* growth at 1

mM (Figure S1), but is toxic at slightly higher levels with a minimal inhibitory concentration (MIC) of ~2.5 mM (Figure S5). The phenotypes we capture therefore reflect effects of sub-MIC doses, which are well known to elicit specific responses, notably secondary metabolite biosynthesis, from bacteria (Goh et al., 2002; Davies et al., 2006; Romero et al., 2011; Seyedsayamdost 2014; Okada and Seyedsayamdost, 2017).

ROS and roseobacticide biosynthesis

We sought to directly search for agents of oxidative stress upon pCA treatment and to examine the effect of these on roseobacticide biosynthesis. First, using a fluorescent dye that exhibits turn-on fluorescence in response to a diverse range of ROS (Oparka et al., 2016), we detected ROS formation that was pCA dose dependent (Figure 5A). At 1 mM pCA, 4-fold greater fluorescence emission was recorded relative to vehicle control, compared with ~9-fold induction with 40 mM H_2O_2, suggesting a significant degree of ROS production with pCA. Likewise, sinapic acid also triggered ROS production, although to a lesser degree, consistent with its diminished effect on *P. inhibens* growth relative to pCA (Figure S1). In the presence of dithiothreitol (DTT), which acts as a reductant *in vivo* (Mashruwala and Bassler, 2020), ROS formation was diminished, again in a dose-dependent manner (Figure 5B). Importantly, a similar trend was observed when measuring roseobacticide synthesis: pCA treatment led to roseobacticide production, but decreased roseobacticide yields were observed with increasing titers of DTT (Figures 5C and 5D), thus correlating roseobacticide yields with ROS levels. While the mechanism underlying this correlation remains to be examined, it is consistent with a model in which pCA triggers roseobacticide biosynthesis via ROS formation and the oxidative stress response. Further studies are necessary to define the role of well-known transcriptional regulators, which facilitate the oxidative stress response (Farr and Kogoma, 1991; Storz and Imlay, 1999), in roseobacticide biosynthesis.

Effect of pCA on energy generation and motility-related genes

Among highly downregulated genes (>3-fold reduction), four subgroups stood out: the first two are essential for chemolithotrophic functions, including reduced sulfur oxidation and carbon monoxide (CO) fixation (Table S7). The other two belong to the pathways of flagellar biosynthesis and chemotaxis. Some *Roseobacter* are capable of chemolithotrophic growth, an adaptation to the nutrient-poor conditions of the pelagic zone (Moran et al., 2004). For example, *Silicibacter pomeroyi* contains a full complement of genes for the oxidation of CO and inorganic sulfur, thereby allowing it to derive energy from these substrates. Although no chemolithotrophic ability has been reported for *P. inhibens* 2.10, it is possible that its full set of CO dehydrogenases and *sox* genes, which encode thiosulfate oxidase homologous to that of *S. pomeroyi*, could add an alternative route for energy generation. The pCA-mediated downregulation of these genes (2.8–14.9-fold) suggests an effect on the overall energy supply in the cell.

To examine this issue further, we carried out primary metabolite analysis and directly measured the levels of nucleotides as well as glycolysis and TCA cycle intermediates using HPLC-MS-based detection (Melamud et al., 2010). We found that NTP levels decreased 2.5–3.1-fold after pCA treatment, consistent with the transcriptomic results (Table 1). Other nucleotides (NMPs and NDPs) that we could detect also registered lower across

the board, between 1.5- and 2.9-fold. Some glycolysis and TCA cycle intermediates experienced a significant decrease, notably glucose-6-phosphate, phosphoenolpyruvate, and acetyl coenzyme A (CoA). Diminution of nicotinamide adenine dinucleotide levels (NAD(P) and NADPH, each down approximately 2-fold) were in line with this notion. Together, the transcriptomic and primary metabolomic results suggest a decrease in cellular energy pools in response to pCA, a condition that is consistent with onset of oxidative stress (Dukan and Nyström, 1999; Imlay, 2019).

Decreased expression of motility-related genes may be related to reduced cellular energy pools, as it has long been known that flagellar activity is governed by the proton motive force (PMF) (Gabel and Berg, 2003). Moreover, downregulation of energy-demanding flagellar and chemotaxis regulons has previously been reported in *Escherichia coli* during oxidative stress (Maurer et al., 2005; Nachin et al., 2005). Indeed, in *P. inhibens* 2.10, expression of *motA* and *motB*, flagellar motor proteins powered by the PMF, as well as expression of many other flagellar and chemotaxis components, were down 3.1–4.2-fold (Table S7). A model connecting energy pools, motility, oxidative stress, and secondary metabolism is discussed further below.

DISCUSSION

Phenylpropanoids are functionally versatile metabolites. In plants, antioxidant activities have been attributed to pCA and other members of this compound family (Korkina, 2007). In *Candida albicans* and neuroblastoma N2a cells, however, pCA treatment leads to oxidative stress (Khan et al., 2011; Shailasree et al., 2015), while antibacterial activities have been described against diverse bacteria (Chesson et al., 1982; Campos et al., 2003; Lou et al., 2012). With *P. inhibens*, we find that pCA is weakly antibiotic, with an MIC of ~2.5 mM. At sub-inhibitory doses, it induces ROS production and global transcriptomic alterations. Most notable among these is induction of secondary metabolism, possibly via the oxidative stress response. Three hallmarks of defense against oxidative stress are evident in the pCA-challenged transcriptome of *P. inhibens* 2.10, production of metal chelators, expression of antioxidant enzymes, and stimulated repair or biosynthesis of essential biopolymers. It was recently shown that *P. inhibens* kills *E. huxleyi* by inducing oxidative stress and ultimately apoptosis-like programmed cell death (Mayers et al., 2016; Segev et al., 2016; Bramucci and Case, 2019). Our results herein show that algal pCA has a very similar impact on *P. inhibens*. Thus, while the two symbionts exchange beneficial metabolites during the mutualistic phase of the symbiosis (Figure 1), the parasitic phase is marked by each partner imparting oxidative damage onto the other using endogenous secondary metabolites.

The transcriptomic results allowed us to identify and characterize roseobactin, a novel siderophore, synthesized by the *rbt* gene cluster in *P. inhibens* 2.10. This molecule adds an additional word to the algal-bacterial dialogue and indicates that *P. inhibens* 2.10 turns on biosynthesis of iron-scavenging metabolites during the parasitic phase of the interaction. The chloroplast and mitochondrion are rich sources of iron as photosynthesis and respiration use a slew of metalloenzymes with iron cofactors. With the production of roseobactin, the bacteria likely secure any iron that is released from dying algal cells as iron is one of the limiting nutrients in the open ocean due to its low solubility (Hider and Kong, 2010). The

production of roseobactin also brings the tally of novel metabolite groups from *P. inhibens* to four. These include TDA, roseobacticides, roseochelins, and roseobactin. Interestingly, *P. inhibens* is not a prolific strain by bioinformatic standards (Thole et al., 2012). However, using an ecology-based strategy, we have continued to find new secondary metabolites and their functions, which together have furthered our understanding of this symbiotic relationship in laboratory studies. These insights provide hypotheses that may be tested in mesocosm or field experiments.

It is tempting to link the transcriptomic responses that we see into a narrative. In this narrative, pCA imparts oxidative stress, which sets into motion the oxidative stress response, allowing the cell to repair damaged biopolymers and mount a secondary metabolite response. The energy for these processes may be obtained by shutting down non-essential processes, such as production of macromolecular machines associated with motility and flagellar locomotion. This rewired energy may then be used to synthesize secondary metabolites, such as roseobactin and roseobacticides, via oxidative stress. These connections, however, were not demonstrated in our study and further work is necessary. It will be interesting to examine the roles of well-known oxidative stress response transcriptional regulators such as OxyR and SoxR in induction of *tda*, *rbt*, and other loci (Farr and Kogoma, 1991; Storz and Imlay, 1999). An alternative model is one where ROS and stimulated secondary metabolite synthesis are parallel responses, both independent consequences of pCA treatment. Distinction between these and other plausible models will be the topic of future work as well as the possibility of energetic rewiring from motility and locomotion to secondary metabolism. Perhaps the more interesting implication here is that *P. inhibens* 2.10 does not “run” when it encounters pCA-mediated oxidative stress. Rather, it “hunkers down” and fights back using small molecule chemical defense, thereby deciding the outcome of a once-mutualistic relationship in its favor.

STAR★METHODS

RESOURCE AVAILABILITY

Lead contact—Further information and requests for resources and reagents should be directed to and will be fulfilled by the lead contact, Mohammad Seyedsayamdost (mrseyed@princeton.edu)

Materials availability—The unique strains (*P. inhibens* 2.10 *ΔpaaC*, *ΔpatB*, *ΔrbtB*, *ΔtdaA*, and *ΔtdaD*) generated in this study are available from the lead contact.

Data and code availability

- Normalized microarray data have been deposited at Mendeley Data and are publicly available as of the date of publication. Accession numbers are listed in the key resources table.
- All original code has been deposited at Mendeley Data and is publicly available as of the date of publication. DOIs are listed in the key resources table.

- Any additional information required to reanalyze the data reported in this paper is available from the lead contact upon request.

EXPERIMENTAL MODEL AND SUBJECT DETAILS

Bacterial strains and growth conditions—*P. inhibens* 2.10 was used throughout this study. It was routinely cultured in ½YTSS medium (per L: 20 g Sigma sea salt, 2 g yeast extract, 1.25 g tryptone) or MB medium (BD 279110). Overnight cultures of *P. inhibens* 2.10 were prepared in 14 mL sterile culture tubes containing 5 mL of ½YTSS medium and incubated at 30°C/250 rpm. Medium and large cultures were grown in ½YTSS medium in Erlenmeyer flasks and incubated at 30°C/160 rpm. *E. coli* DH5α cells (NEB), used for cloning, were routinely cultured in LB (Fisher BP97235) medium. Antibiotics were used at 50 μg/mL (kanamycin) and 25 μg/mL (gentamicin) for both strains. pCA was prepared as a 100 mM stock in 1:1 water/MeCN throughout these experiments. The additional of pCA, to a final concentration of 1 mM did not significantly affect the pH of the medium. Innocula were quantified spectroscopically using a previously determined conversion factor (OD_{600} = 1 corresponds to 1.0 ± 0.2 10^9 cells/mL). To identify roseobactin, ½YTSS medium supplemented with a final concentration of 100 μM EDTA, which was added from a pH-adjusted stock (7.5) and did not alter the pH of the medium.

METHOD DETAILS

HPLC, HPLC-MS, and NMR spectroscopy—HPLC purifications were carried out on an Agilent 1200 Series analytical HPLC system equipped with a photo diode array detector and an automated fraction collector, or on an Agilent 1200 Series preparative HPLC system also equipped with the same modules. Low resolution HPLC-ESI-MS analysis was performed on an Agilent 1200 Series HPLC system equipped with a diode array detector and a 6130 Series ESI mass spectrometer using an analytical Phenomenex Luna C18 column (5 μm, 4.6 × 100 mm) operating at 0.5 mL/min with a gradient of 25% MeCN in H_2O (+0.1% formic acid, FA) to 100% MeCN (+0.1% FA) over 20 min. High resolution (HR) ESI-MS and HR-tandem MS (HR-MS/MS) were carried out on a 6540 UHD Accurate Mass Q-tof HPLC-MS system (Agilent), equipped with a 1260 Infinity Series HPLC, an automated liquid sampler, a diode array detector, a JetStream ESI source, and the 6540 Series Q-tof. The ESI-MS was calibrated to within 1 ppm prior to analysis, and samples were resolved on an Agilent C18 Eclipse column (2.7 μm, 3 × 50 mm) at a flow rate of 0.4 mL/min using water and MeCN as mobile phases (plus 0.1% FA). ^{1}H and 2D NMR spectra were recorded at the Princeton Chemistry NMR Core Facility on a Bruker Avance III 500 MHz spectrometer equipped with a ^{1}H-optimized cryoprobe. Roseobactin NMR spectra were obtained in D_2O and 9:1 H_2O/D_2O; chemical shifts were referenced to the residual solvent peak.

Molecular biology—Genomic DNA was isolated using the Wizard gDNA Isolation Kit (Promega). Primers were purchased from Sigma-Aldrich. PCR reactions were performed with Q5 high-fidelity DNA polymerase (NEB) for cloning and genetic manipulations, and with Taq DNA polymerase (NEB) for knockout validation. Restriction enzymes and T4 DNA ligase were purchased from NEB. PCR purification and agarose gel extraction were carried out with Qiagen kits.

Microarray analysis—*P. inhibens* 2.10 microarray was constructed using the Agilent eArray tool (https://earray.chem.agilent.com/earray). Three probes were chosen for each open reading frame and arrayed by the manufacturer. For the microarray experiment, *P. inhibens* 2.10 was grown in a sterile 14 mL tube containing 5 mL ½YTSS at 30°C/250 rpm overnight. The overnight culture was diluted into 15 mL ½YTSS medium in a 125 mL flask with 1 mM pCA or without pCA, containing only the same volume of the vehicle, at a starting optical density at 600 nm (OD_{600}) of 0.05. Biological triplicates were used for each condition. The cultures were grown for 24 hr to early stationary phase, and 200 μL from each growth was used for total RNA isolation via the RNeasy minikit (Qiagen), followed by removal of contaminating DNA with the DNAfree kit (Ambion). RNA concentrations were measured using an H1MF plate reader (Biotek) and the presence of intact RNA was verified using an Agilent Bioanalyzer 2100 in the Microarray Core Facility at Princeton University. 100 ng of total RNA was used from each replicate for further processing. RNA samples were first reverse-transcribed to cDNA using the Agilent Quick Amp Labeling Kit. cDNA was then transcribed to cRNA using T7 RNA polymerase (Agilent) with cyanine 5–cytidine-5′-triphosphate (Cy5-CTP, Enzo Life Sciences) labeling the pCA-treated samples and cyanine 3–cytidine-5′-triphosphate (Cy3-CTP, Enzo Life Sciences) labeling the control samples. After a cleanup step using the Qiagen RNeasy minikit, cRNA yields and dye incorporation were quantified using a Nanodrop ND-1000 spectrophotometer. 300 ng of cRNA was used for microarray library construction with optimal dye incorporation of 15 pmol for each sample. Libraries were constructed by fragmenting the experimental and control samples using the Agilent Gene Expression Hybridization Kit. RNA libraries were then combined and hybridized to the microarray chip for 17 hr at 65°C with gentle agitation at 10 rpm. The microarray chip was washed twice with Agilent wash buffer 1 and 2 and then dried with MeCN. The chip was scanned by an Agilent G2505B scanner and the readout was extracted from the scanned TIFF image using Agilent Feature Extract software. Extracted data was uploaded to the Princeton University Microarray Analysis database (PUMAdb) for archiving. Significance Analysis for Microarray (SAM) was carried out in R package, version 4.01. The statistics embedded in the R package included a non-parametric test with FDR (false discovery rate).

Primary metabolite analysis—Primary metabolomics was carried out as previously described (Melamud et al., 2010). Briefly, *P. inhibens* 2.10 was grown in 14 mL sterile culture tubes containing 5 mL of ½YTSS at 30°C/250 rpm overnight. The culture was diluted into 15 mL ½YTSS medium in a 125 mL flask with and without 1 mM pCA starting at an OD_{600} of 0.05 in triplicates for each condition. After 24 hr, OD_{600} was measured and 1 mL of culture from each replicate was filtered through a 50 mm nylon membrane and immediately quenched in 3 mL of extraction solvent (2:2:1 MeCN:MeOH:H_2O with 0.1 M FA). Extracts were neutralized with 225 μL of 15% (w/v) NH_4HCO_3, transferred to 1.5 mL Eppendorf tubes, and centrifuged at maximum speed for 10 min. 800 μL of supernatant from each sample was dried in vacuo and resuspended in 110 μL H_2O. 10 μL of each sample was analyzed by a reverse-phase ion-pairing liquid chromatography coupled to a high-resolution, high-accuracy QExactive mass spectrometer (Thermo). Metabolites were quantified in MAVEN software (Melamud et al., 2010) using integrated peak areas

from extracted ion chromatograms and averaged for triplicates. Fold-change relative to the untreated samples was determined for all metabolites detected.

Creation of targeted gene deletion mutants—Targeted gene deletions were carried out as previously described (Wang et al., 2016). Briefly, for each deletion, a knockout plasmid was constructed by inserting a knockout cassette, consisting of a gentamicin resistance gene cloned from pEX18Gm-pheS flanked by at least 1 kb DNA sequence upstream and downstream of the target gene, into the parent plasmid pRW01. At least 1 μg of knock out plasmid was transformed into *P. inhibens* 2.10 by electroporation as described before (Wang et al., 2016). Cells were selected on ½MB agar plates containing 25 μg/mL gentamicin, followed by a counter selection on ½YTSS agar plates containing 0.1% p-Cl-phenylalanine. Mutants were verified by colony PCR and sequencing. Primers used for mutant generation and verification are shown (Table S2). Primers 1 and 2 were used for amplifying the upstream region of the target gene, while primers 3 and 4 were used for amplifying the downstream region.

Quantitative RT-PCR—*P. inhibens* 2.10 was grown in 5 mL ½YTSS at 30°C/250 rpm in a 14 mL culture tube overnight. The culture was diluted into 15 mL ½YTSS medium in a 125 mL flask with 1 mM pCA and without, containing the same volume of the vehicle, at a starting OD_{600} of 0.05. Three biological replicates were used for each condition. After 24 hr, the OD_{600} was measured and related to cell counts using the conversion factor OD_{600} of 1 = 10^9 cells/mL. This conversion factor was determined by serial dilution and cell counting. 200 μL of each culture was then used for total RNA isolation. Residual DNA was removed using the Ambion DNAfree kit. Finally, about 400–500 ng of RNA was converted into cDNA using the Bio-Rad iScript kit.

Two genes, *rbtA* (PGA2_95p500) and *rbtE* (PGA2_95p540), in the *rbt* gene cluster were chosen for quantification by RT-qPCR as well as the 16S rRNA gene. Using the primer-3-plus software, the primers were designed to give an amplicon length of 120–150 bp and a melting temperature of 85–90°C, as well as a G/C-clamp at the 3′ end. Each amplicon was amplified by PCR using Q5 DNA polymerase and purified by gel extraction. A series of standards were generated for each amplicon ranging from 100 ag/μL to 100 pg/μL in 10-fold dilutions. These served as standards for quantification of the same amplicons from the experimental samples.

qPCR analysis was performed on a Bio-Rad CFX96 Real-Time PCR Detection System. The reaction was carried out in hard-shell, clear 96-well qPCR plates (Bio-Rad) and utilized the iTaq Universal SYBR Green Supermix (Bio-Rad). In a total volume of 16 μL, each well contained 8 μL of iTaq Supermix, 1 μL of standard DNA or cDNA, 1 or 2 μL of 10 μM primer mix (optimized for quantification for each amplicon) and 5 μL or 4 μL of nuclease-free water. The PCR cycle consisted of a 1-min incubation at 95°C followed by 42 cycles of a 2-step amplification protocol (5 s at 95°C, then 30 s at annealing/extension temperature). Finally, a denaturation cycle was applied to determine the melting temperature of the amplicon, where a single species was observed in all experiments.

qPCR conditions for each gene were optimized with the amplicon standard DNA generated above as template, by first varying the primer concentration and then the annealing/extension temperature, which ranged from 50 to 60°C in eight steps. The combination that gave the lowest quantification cycle (Cq) and highest fluorescence were used in the experiments. A standard curve was generated by plotting the average Cq (from duplicate standards) against the log of a series of standard amplicon DNA from 1 pg/μL to 100 ag/μL. To determine the levels of each transcript as a function of pCA, the Cq for each sample was determined in triplicates and converted back to amplicon concentration using the standard curve. The resulting value was then normalized for total cells used in the RNA isolation step and further normalized to the vehicle control to give fold-change.

Roseobacticide and TDA detection—*P. inhibens* 2.10 cultures were cultured in 20mL 1/2YTSS medium with or without 1mM pCA for 3 days. Each culture was extracted with 2 volumes of ETOAc (supplemented with .1% formic acid for TDA) and the organic layer was dried *in vacuo*. and resuspended with 600μL MeOH. 10μL of each sample was analyzed by LC/MS with a column gradient as mentioned above. Roseobacticides were quantified by integrating the UV 430nm absorption. TDA was quantified by integrating the UV 304nm absorption.

Siderophore detection—Wild-type *P. inhibens* 2.10 and the *rbtB::gnt* insertional inactivation mutant were cultured in 20 mL ½YTSS medium supplemented with a final concentration of 100 μM EDTA for 2 days. The filtered culture supernatants were applied to Oasis HLB solid-phase extraction columns (150 mg sorbent, 6 mL syringe), which had been washed with 10 column volumes (CV) of MeOH and equilibrated with 10 CV of H_2O. After loading, the material was eluted with 2 mL of 5% MeOH, and eluted with 2 mL of 50% MeOH and 2 mL of 100% MeOH. 100 μL of each fraction was analyzed using the CAS assay as previously reported to identify siderophore-containing fraction(s) (Schwyn and Neilands 1987). HR-MS/MS experiments were also carried out on the supernatants: the filtered culture supernatant was applied to an Oasis Max column (10 mg sorbent, 1 mL syringe), which had been washed with 10 CV of MeOH and 10 CV of H_2O, and eluted with 5 mL of MeOH followed by 5 mL of MeOH +0.2% FA. Both fractions were dried in vacuo and resuspended in 500 μL of 50% MeOH. 10 μL of each fraction was analyzed with an HPLC-Qtof-MS with column gradient of 5% MeCN in H_2O (+0.1% FA) to 95% MeCN in H_2O (+0.1% FA) over 37 min. HR-MS/MS data were collected under positive ion detection mode using collision energies at 30 V and 50 V, a scan rate of 3 spectra per second, and a spectral range of 100-2000 m/z. A product ion of *m/z* 137.02 was used to search for potential catechol-containing siderophores.

Roseobactin isolation—*P. inhibens* 2.10 was grown in 5 mL ½YTSS at 30°C/250 rpm overnight. The overnight culture was diluted into 15 mL ½YTSS medium in a 125 mL flask and grown at 30°C/160 rpm for 20 hr before diluting into large cultures. Large cultures (6 × 800 mL in 4 L flask) of *P. inhibens* 2.10 were grown in ½YTSS supplemented with 100 μM EDTA and 1 mM pCA, starting with an initial $OD_{600\ nm}$ of 0.05 at 30°C/160 rpm. After 2 days, at which point roseobactin production was optimal, the large cultures were spun down and the supernatant filtered prior to application to an Oasis HLB column (1 g sorbent,

20 mL syringe), which had been washed with 10 CV of MeOH and equilibrated with 10 CV of H_2O. The HLB column was washed with 50 mL of 5% MeOH, and then eluted stepwise with 25 mL each of 20%, 40%, 70%, and 100% MeOH plus 0.2% FA. The 20% fraction, which contained roseobactin, was dried down in vacuo and subsequently separated by preparative HPLC using a Phenomenex Luna C18 column (5 μm, 21.2 × 250 mm) with a gradient of 5–59% MeCN in H_2O + 0.1% FA over 21 min. The fractions containing roseobactin were combined and dried in vacuo. A second separation on semi-preparative HPLC using a Phenomenex Luna C18 column (5 μm, 10 × 250 mm) with an isocratic gradient of 7% MeCN in H_2O (+0.1% FA) delivered pure roseobactin.

ROS detection—Chloromethyl-H_2DCFDA (ThermoFisher) was used to detect ROS (Oparka et al., 2016). *P. inhibens* 2.10 was grown in a sterile 14 mL tube containing 5 mL ½YTSS at 30°C/250 rpm overnight. These were then diluted into 25 mL ½YTSS medium in a 125 mL flask with and without added compound of interest. Cultures were grown at 30°C/160 rpm for ~10 hr to an OD_{600} ~1. Dye was added to the culture to a final concentration of 10 μM. Cultures were incubated at 30°C/160 rpm in the dark for 30 min after which point 200 μL of each culture was spun down, washed twice, and resuspended in 100 μL 1x PBS buffer. Fluorescence emission was measured using a Biotek H1MF microplate reader with an excitation wavelength (λ_{ex}) set to 495 nm, and emission wavelength (λ_{em}) set to 525 nm. The fluorescence intensities measured were normalized for OD_{600}.

QUANTIFICATION AND STATISTICAL ANALYSIS

The arithmetic mean and standard deviation across multiple biological replicates were our measures of center and spread. Details of replicates and data analysis for each experiment can be found in the figure legends. GraphPad Prism 9 and R were used for statistical analysis. Unpaired two-tailed t-tests were used for significance between two treatment groups.

Supplementary Material

Refer to Web version on PubMed Central for supplementary material.

ACKNOWLEDGMENTS

We thank the Burroughs Wellcome Fund (PATH Investigator Award to M.R.S.), the National Institutes of Health (grant 1DP1OD019133 to Z.G.), the Princeton Catalysis Initiative (joint grant to Z.G. and M.R.S.), and the China Scholarship Council (graduate fellowship to A.L.), for support of this work.

REFERENCES

Abergel RJ, Zawadzka AM, and Raymond KN (2008). Petrobactin-mediated iron transport in pathogenic bacteria: coordination chemistry of an unusual 3,4-catecholate/citrate siderophore. J. Am. Chem. Soc 130, 2124–2125. [PubMed: 18220393]

Barbeau K, Zhang G, Live DH, and Butler A (2002). Petrobactin, a photo-reactive siderophore produced by the oil-degrading marine bacterium *Marinobacter hydrocarbonoclasticus*. J. Am. Chem. Soc 124, 378–379. [PubMed: 11792199]

Barrett AR, Kang Y, Inamasu KS, Son MS, Vukovich JM, and Hoang TT (2008). Genetic tools for allelic replacement in *Burkholderia species*. Appl. Environ. Microbiol 74, 4498–4508. [PubMed: 18502918]

Berger M, Neumann A, Schulz S, Simon M, and Brinkhoff T (2011). Tropodithietic acid production in *Phaeobacter gallaeciensis* is regulated by N-acyl homoserine lactone-mediated quorum sensing. J. Bacteriol 193, 6576–6585. [PubMed: 21949069]

Bramucci AR, and Case RJ (2019). *Phaeobacter inhibens* induces apoptosis-like programmed cell death in calcifying *Emiliania huxleyi*. Sci. Rep 9, 5215. [PubMed: 30894549]

Brinkhoff T, Bach G, Heidorn T, Liang L, Schlingloff A, and Simon M (2004). Antibiotic production by a *Roseobacter* clade-affiliated species from the German Wadden Sea and its antagonistic effects on indigenous isolates. Appl. Environ. Microbiol 70, 2560–2565. [PubMed: 15066861]

Brinkhoff T, Giebel H-A, and Simon M (2008). Diversity, ecology and genomics of the *Roseobacter* clade: a short overview. Arch. Microbiol 189, 531–539. [PubMed: 18253713]

Bruhn JB, Nielsen KF, Hjelm M, Hansen M, Bresciani J, Schulz S, and Gram L (2005). Ecology, inhibitory activity, and morphogenesis of a marine antagonistic bacterium belonging to the *Roseobacter* clade. Appl. Environ. Microbiol 71, 7263–7270. [PubMed: 16269767]

Buchan A, González JM, and Moran MA (2005). Overview of the marine *Roseobacter* lineage. Appl. Environ. Microbiol 71, 5665–5677. [PubMed: 16204474]

Campos FM, Couto JA, and Hogg TA (2003). Influence of phenolic acids on growth and inactivation of Oenococcus oeni and *Lactobacillus hilgardii*. J. Appl. Microbiol 94, 167–174. [PubMed: 12534807]

Challis GL (2005).Awidelydistributed bacterial pathway for siderophore biosynthesis independent of nonribosomal peptide synthetases. ChemBioChem 6, 601–611. [PubMed: 15719346]

Chen JW, Dodia C, Feinstein SI, Jain MK, and Fisher AB (2000). 1-Cys peroxiredoxin, a bifunctional enzyme with glutathione peroxidase and phospholipase A2 activities. J. Biol. Chem 275, 28421–28427. [PubMed: 10893423]

Chesson A, Stewart CS, and Wallace RJ (1982). Influence of plant phenolic acids on growth and cellulolytic activity of rumen bacteria. Appl. Environ. Microbiol 44, 597–603. [PubMed: 16346090]

Davies J, Spiegelman GB, and Yim G (2006). The world of subinhibitory antibiotic concentrations. Curr. Opin. Microbiol 9, 445–453. [PubMed: 16942902]

Dogs M, Voget S, Teshima H, Petersen J, Davenport K, Dalingault H, Chen A, Pati A, Ivanova N, Goodwin LA, et al. (2013). Genome sequence of *Phaeobacter inhibens* type strain T5, a secondary metabolite producing representative of the marine *Roseobacter* clade, and emendation of the species description of *Phaeobacter inhibens*. Stand. Genomic Sci 9, 334–350. [PubMed: 24976890]

Dukan S, and Nyström T (1999). Oxidative stress defense and deterioration of growth-arrested *Escherichia coli* cells. J. Biol. Chem 274, 26027–26032. [PubMed: 10473549]

Espiñeira JM, Novo Uzal E, Gómez Ros LV, Carrión JS, Merino F, Ros Barceló A, and Pomar F (2011). Distribution of lignin monomers and the evolution of lignification among lower plants. Plant Biol. 13, 59–68. [PubMed: 21143726]

Farr SB, and Kogoma T (1991). Oxidative stress responses in *Escherichia coli* and *Salmonella typhimurium*. Microbiol. Rev 55, 561–585. [PubMed: 1779927]

Gabel CV, and Berg HC (2003). The speed of the flagellar rotary motor of *Escherichia coli* varies linearly with protonmotive force. Proc. Natl. Acad. Sci. U S A 100, 8748–8751. [PubMed: 12857945]

Geng H, Bruhn JB, Nielsen KF, Gram L, and Belas R (2008). Genetic dissection of tropodithietic acid biosynthesis by marine roseobacters. Appl. Environ. Microbiol 74, 1535–1545. [PubMed: 18192410]

Geng H, and Belas R (2010). Molecular mechanisms underlying *Roseobacter*-phytoplankton symbioses. Curr. Opin. Biotechnol 21, 332–338. [PubMed: 20399092]

Goh E-B, Yim G, Tsui W, McClure J, Surette MG, and Davies J (2002). Transcriptional modulation of bacterial gene expression by subinhibitory concentrations of antibiotics. Proc. Natl. Acad. Sci. U S A 99, 17025–17030. [PubMed: 12482953]

González JM, Kiene RP, and Moran MA (1999). Transformation of sulfur compounds by an abundant lineage of marine bacteria in the alpha-subclass of the class Proteobacteria. Appl. Environ. Microbiol 65, 3810–3819. [PubMed: 10473380]

Hagan AK, Plotnick YM, Dingle RE, Mendel ZI, Cendrowski SR, Sherman DH, Tripathi A, and Hanna PC (2018). Petrobactin protects against oxidative stress and enhances sporulation efficiency in *Bacillus anthracis* Sterne. mBio 9, e02079–18. [PubMed: 30401780]

Hider RC, and Kong X (2010). Chemistry and biology of siderophores. Nat. Prod. Rep 27, 637–657. [PubMed: 20376388]

Hogle SL, Barbeau KA, and Gledhill M (2014). Heme in the marine environment: from cells to the iron cycle. Metallomics 6, 1107–1120. [PubMed: 24811388]

Huerta-Cepas J, Forslund K, Coelho LP, Szklarczyk D, Jensen LJ, von Mering C, and Bork P (2017). Fast genome-wide functional annotation through orthology assignment by eggnog-mapper. Mol. Biol. Evol 34, 2115–2122. [PubMed: 28460117]

Imlay JA (2019). Where in the world do bacteria experience oxidative stress? Environ. Microbiol 21, 521–530. [PubMed: 30307099]

Khan A, Ahmad A, Akhtar F, Yousuf S, Xess I, Khan LA, and Manzoor N (2011). Induction of oxidative stress as a possible mechanism of the antifungal action of three phenylpropanoids. FEMS Yeast Res. 11, 114–122. [PubMed: 21114624]

Koppisch AT, Dhungana S, Hill KK, Boukhalfa H, Heine HS, Colip LA, Romero RB, Shou Y, Ticknor LO, Marrone BL, et al. (2008). Petrobactin is produced by both pathogenic and non-pathogenic isolates of the *Bacillus cereus* group of bacteria. Biometals 21, 581–589. [PubMed: 18459058]

Korkina LG (2007). Phenylpropanoids as naturally occurring antioxidants: from plant defense to human health. Cell. Mol. Biol 53, 15–25.

Kvint K, Nachin L, Diez A, and Nyström T (2004). The bacterial universal stress protein: function and regulation. Curr. Opin. Microbiol 6, 140–145.

Lee JY, Janes BK, Passalacqua KD, Pfleger BF, Bergman NH, Liu H, Håkansson K, Somu RV, Aldrich CC, Cendrowski S, et al. (2007). Biosynthetic analysis of the petrobactin siderophore pathway from *Bacillus anthracis*. J. Bacteriol 189, 1698–1710. [PubMed: 17189355]

Lou Z, Wang H, Rao S, Sun J, Ma C, and Li J (2012). p-Coumaric acid kills bacteria through dual damage mechanisms. Food Control 25, 550–554.

Mashruwala AA, and Bassler BL (2020). The *Vibrio cholerae* quorum-sensing protein VqmA integrates cell density, environmental, and host-derived cues into the control of virulence. mBio 11, e01572–20. [PubMed: 32723922]

Martone PT, Estevez JM, Lu F, Ruel K, Denny MW, Somerville C, and Ralph J (2009). Discovery of lignin in seaweed reveals convergent evolution of cell-wall architecture. Curr. Biol 19, 169–175. [PubMed: 19167225]

Maurer LM, Yohannes E, Bondurant SS, Radmacher M, and Slonczewski JL (2005). pH regulates genes for flagellar motility, catabolism, and oxidative stress in *Escherichia coli* K-12. J. Bacteriol 187, 304–319. [PubMed: 15601715]

Mayers TJ, Bramucci AR, Yakimovich KM, and Case RJ (2016). A bacterial pathogen displaying temperature-enhanced virulence of the microalga *Emiliania huxleyi*. Front. Microbiol 7, 892. [PubMed: 27379036]

Melamud E, Vastag L, and Rabinowitz JD (2010). Metabolomic analysis and visualization engine for LCMS data. Anal. Chem 82, 9818–9826. [PubMed: 21049934]

Mishra S, and Imlay J (2012). Why do bacteria use so many enzymes to scavenge hydrogen peroxide? Arch. Biochem. Biophys 525, 145–160. [PubMed: 22609271]

Moran MA, Buchan A, González JM, Heidelberg JF, Whitman WB, Kiene RP, Henriksen JR, King GM, Belas R, Fuqua C, et al. (2004). Genome sequence of *Silicibacter pomeroyi* reveals adaptations to the marine environment. Nature 432, 910–913. [PubMed: 15602564]

Nachin L, Nannmark U, and Nyström T (2005). Differential roles of the universal stress proteins of *Escherichia coli* in oxidative stress resistance, adhesion, and motility. J. Bacteriol 187, 6265–6272. [PubMed: 16159758]

Okada BK, and Seyedsayamdost MR (2017). Antibiotic dialogues: induction of silent biosynthetic gene clusters by exogenous small molecules. FEMS Microbiol. Rev 41, 19–33. [PubMed: 27576366]

Oparka M, Walczak J, Malinska D, van Oppen LMPE, Szczepanowska J, Koopman WJH, and Wieckowski MR (2016). Quantifying ROS levels using CM-H_2DCFDA and HyPer. Methods 109, 3–11. [PubMed: 27302663]

Porsby CH, Nielsen KF, and Gram L (2008). *Phaeobacter* and *Ruegeria* species of the *Roseobacter* clade colonize separate niches in a Danish turbot (*Scophthalmus maximus*)-rearing farm and antagonize *Vibrio anguillarum* under different growth conditions. Appl. Environ. Microbiol 74, 7356–7364. [PubMed: 18952864]

Rao D, Webb JS, and Kjelleberg S (2006). Microbial colonization and competition on the marine alga *Ulva australis*. Appl. Environ. Microbiol 72, 5547–5555. [PubMed: 16885308]

Roe KL, Hogle SL, and Barbeau KA (2013). Utilization of heme as an iron source by marine alphaproteobacteria in the *Roseobacter* clade. Appl. Environ. Microbiol 79, 5753–5762. [PubMed: 23872569]

Romero D, Traxler MF, López D, and Kolter R (2011). Antibiotics as signal molecules. Chem. Rev 111, 5492–5505. [PubMed: 21786783]

Schlacher K, and Goodman MF (2007). Lessons from 50 years of SOS DNA-damage-induced mutagenesis. Nat. Rev. Mol. Cell Biol 8, 587–594. [PubMed: 17551516]

Schwyn B, and Neilands JB (1987). Universal chemical assay for the detection and determination of siderophores. Anal. Biochem 160, 47–56. [PubMed: 2952030]

Seyedsayamdost MR, Case RJ, Kolter R, and Clardy J (2011a). The Jekyll-and-Hyde chemistry of *Phaeobacter gallaeciensis*. Nat. Chem 3, 331–335. [PubMed: 21430694]

Seyedsayamdost MR, Carr G, Kolter R, and Clardy J (2011b). Roseobacticides: small molecule modulators of an algal-bacterial symbioses. J. Am. Chem. Soc 133, 18343–18349. [PubMed: 21928816]

Seyedsayamdost MR, Wang R, Kolter R, and Clardy J (2014). Hybrid biosynthesis of roseobacticides from algal and bacterial precursor molecules. J. Am. Chem. Soc 136, 15150–15153. [PubMed: 25295497]

Segev E, Wyche TP, Kim KH, Petersen J, Ellebrandt C, Vlamakis H, Barteneva N, Paulson JN, Chai L, Clardy J, and Kolter R (2016). Dynamic metabolic exchange governs a marine algal-bacterial interaction. eLife 5, e17473. [PubMed: 27855786]

Seyedsayamdost MR (2014). High-throughput platform for the discovery of elicitors of silent bacterial gene clusters. Proc. Natl. Acad. Sci. U S A 111, 7266–7271. [PubMed: 24808135]

Seymour JR, Simó R, Ahmed T, and Stocker R (2010). Chemoattraction to dimethylsulfoniopropionate throughout the marine microbial food web. Science 329, 342–345. [PubMed: 20647471]

Shailasree S, Venkataramana M, Niranjana SR, and Prakash HS (2015). Cytotoxic effect of p-coumaric acid on neuroblastoma, N2a cell via generation of reactive oxygen species leading to dysfunction of mitochondria inducing apoptosis and autophagy. Mol. Neurobiol 51, 119–130. [PubMed: 24760364]

Storz G, and Imlay JA (1999). Oxidative stress. Curr. Opin. Microbiol 2, 188–194. [PubMed: 10322176]

Stubbe J (2000). Ribonucleotide reductases: the link between an RNA and a DNA world? Curr. Opin. Struct. Biol 10, 731–736. [PubMed: 11114511]

Taddei F, Hayakawa H, Bouton M, Cirinesi A, Matic I, Sekiguchi M, and Radman M (1997). Counteraction by MutT protein of transcriptional errors caused by oxidative damage. Science 278, 128–130. [PubMed: 9311918]

Thiel V, Brinkhoff T, Dickschat JS, Wickel S, Grunenberg J, Wagner-Döbler I, Simon M, and Schulz S (2010). Identification and biosynthesis of tropone derivatives and sulfur volatiles produced by bacteria of the marine *Roseobacter* clade. Org. Biomol. Chem 8, 234–246. [PubMed: 20024154]

Thole S, Kalhoefer D, Voget S, Berger M, Engelhardt T, Liesegang H, Wollherr A, Kjelleberg S, Daniel R, Simon M, et al. (2012). *Phaeobacter gallaeciensis* genomes from globally opposite locations reveal high similarity of adaptation to surface life. ISME J. 6, 2229–2244. [PubMed: 22717884]

Tusher VG, Tibshirani R, and Chu G (2001). Significance analysis of microarrays applied to the ionizing radiation response. Proc. Natl. Acad. Sci. U S A 98, 5116–5121. [PubMed: 11309499]

Wagner-Döbler I, and Biebl H (2006). Environmental biology ofthe marine *Roseobacter* lineage. Annu. Rev. Microbiol 60, 255–280. [PubMed: 16719716]

Wagner-Döbler I, Ballhausen B, Berger M, Brinkhoff T, Buchholz I, Bunk B, Cypionka H, Daniel R, Drepper T, Gerdts G, et al. (2010). The complete genome sequence of the algal symbiont *Dinoroseobacter shibae*: a hitch-hiker's guide to life in the sea. ISME J. 4, 61–77. [PubMed: 19741735]

Wang H, Tomasch J, Jarek M, and Wagner-Döbler I (2014). A dual-species co-cultivation system to study the interactions between roseobacters and dinoflagellates. Front. Microbiol 5, 311. [PubMed: 25009539]

Wang H, Tomasch J, Michael V, Bhuju S, Jarek M, Petersen J, and Wagner-Döbler I (2015). Identification of genetic modules mediating the Jekyll and Hyde interaction of *Dinoroseobacter shibae* with the dinoflagellate *Prorocentrum minimum*. Front. Microbiol 6, 1262. [PubMed: 26617596]

Wang R, Gallant E, and Seyedsayamdost MR (2016). Investigation of the genetics and biochemistry of roseobacticide production in the *Roseobacter* clade bacterium *Phaeobacter inhibens*. mBio 7, e02118–15. [PubMed: 27006458]

Wang R, and Seyedsayamdost MR (2017). Roseochelin B, an algaecidal natural product synthesized by *Phaeobacter inhibens* in response to algal sinapic acid. Org. Lett 19, 5138–5141. [PubMed: 28920692]

Wienhausen G, Noriega-Ortega BE, Niggemann J, Dittmar T, and Simon M (2017). The exometabolome of two model strains of the *Roseobacter* group: a marketplace of microbial metabolites. Front. Microbiol 8, 1985. [PubMed: 29075248]

Wilson MZ, Wang R, Gitai Z, and Seyedsayamdost MR (2016). Mode of action and resistance studies unveil new roles for tropodithietic acid as an anti-cancer agent and the g-glutamyl cycle as a proton sink. Proc. Natl. Acad. Sci. U S A 113, 1630–1635. [PubMed: 26802120]

Xiao M, Lai Y, Sun J, Chen G, and Yan A (2016). Transcriptional regulation of the outer membrane porin gene ompW reveals its physiological role during the transition from the aerobic to the anaerobic lifestyle of *Escherichia coli*. Front. Microbiol 7, 799. [PubMed: 27303386]

Zhang Y, Heym B, Allen B, Young D, and Cole S (1992). The catalase-peroxidase gene and isoniazid resistance of *Mycobacterium tuberculosis*. Nature 358, 591–593. [PubMed: 1501713]

Highlights

- Algal *p*-coumaric acid induces cell-wide transcriptional changes in *P. inhibens*
- The most upregulated genes are involved in oxidative stress and secondary metabolism
- Transcriptomic and genetic studies led to the discovery of the siderophore roseobactin
- The effect of *p*-coumaric acid may be mediated through formation of ROS

SIGNIFICANCE

Microbes communicate with a language consisting of small molecules. The molecules can be thought of as words and their functions as meaning. Understanding how microbes interact, therefore, boils down to establishing the lexicon of molecules that are exchanged and elucidating their functions. In this work, we add a new word and its meaning to the algal-bacterial dialogue, a siderophore that we call roseobactin. The cluster coding for roseobactin is induced by algal pCA. Previously thought of as a senescence molecule, our studies show that pCA actually has another, or an additional, function. It is toxic to the bacteria at high concentrations but induces secondary metabolism and the oxidative stress response at sub-lethal doses. Our work sheds light on the parasitic phase of this interaction, one where each symbiont exerts oxidative stress onto the other with a strain-specific armory of metabolites. In *E. huxleyi*, sustained oxidative stress leads to programmed cell death, as previous studies have shown. In *P. inhibens*, oxidative stress correlates with, and perhaps triggers, synthesis of roseobactin and the algaecidal roseobacticides. Aside from these specific insights, our work underlines the advantages of interrogating symbiotic interactions as sources of new natural products. It also consolidates algal-bacterial interactions as simplified model systems for more complex bacterial-eukaryote associations that occur in microbially dense environments such as soil or mammalian microbiomes.

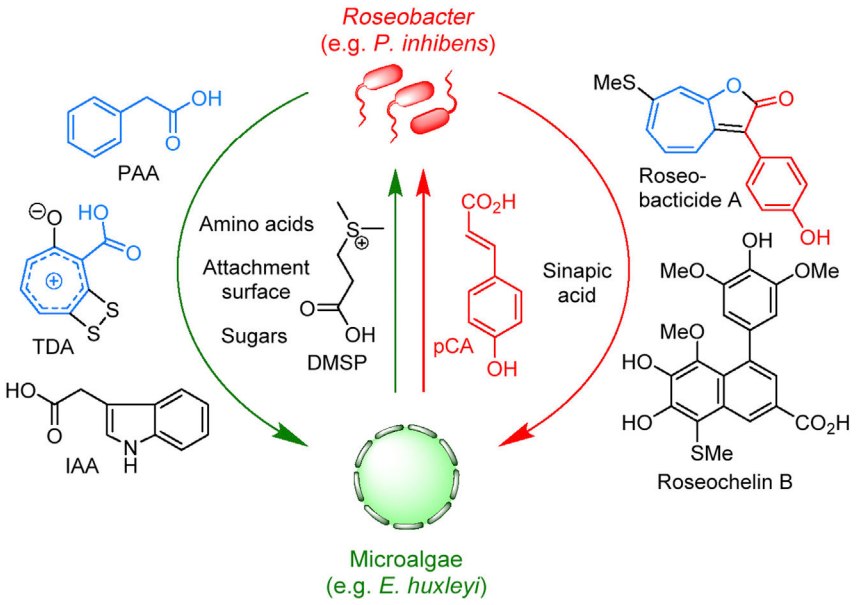

Figure 1. Current model for microalgal-bacterial symbioses

The symbiosis is biphasic, indicated by green and red arrows for the mutualistic and parasitic phases, respectively. During the mutualistic phase, beneficial metabolites are exchanged. The microalgae provide nutrients, such as amino acids, sugars, and DMSP, as well as an attachment surface. The bacteria in return produce the auxins phenylacetic acid (PAA) and indole-3-acetic acid (IAA), the protective metabolite TDA, and likely vitamins (not shown). In the parasitic phase, microalgae release phenylpropanoids; *E. huxleyi* has been shown to produce pCA, while other algae produce sinapic acid. In response to pCA, *P. inhibens* produces the toxic roseobacticides, which are synthesized from PAA and pCA (as color coded). Sinapic acid elicits both roseobacticides and roseochelin B.

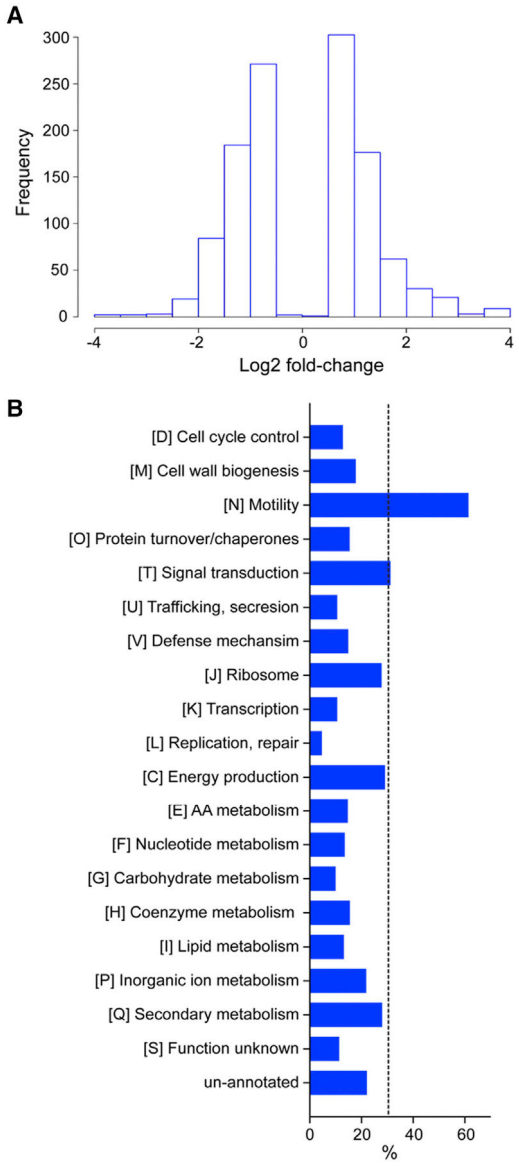

Figure 2. Transcriptomic analysis of *P. inhibens* 2.10 in response to pCA

(A) Histogram of significantly expressed genes in pCA-treated *P. inhibens* 2.10 cells as determined by microarray analysis.

(B) EggNOG analysis: shown are the percentage of genes within each indicated pathway for which expression was altered >2-fold. The dotted line marks 30%.

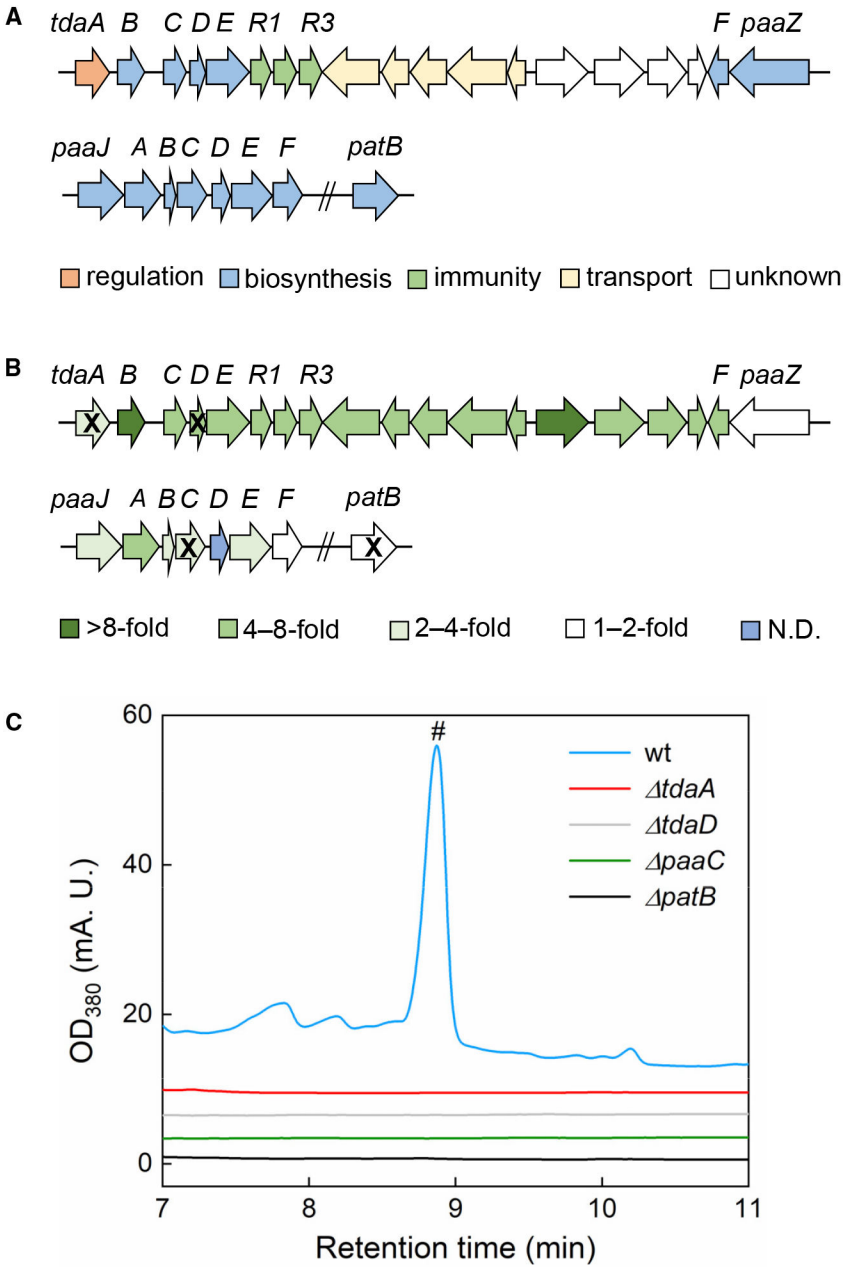

Figure 3. pCA transcriptionally induces the *tda* and *paa* gene clusters

(A) Arrangement of *tda*, *paa*, and *patB* in *P. inhibens* 2.10. Genes are color coded as shown.

(B) Induction of the *tda* cluster. Genes are color coded according to induction level in the presence of pCA (see also Table S4). Genes deleted by mutagenesis in follow-up studies are marked with an X.

(C) Genes within the *tda* and *paa* operons as well as *patB* are required for roseobacticide biosynthesis in *P. inhibens* 2.10. Shown are HPLC-MS traces of the induced metabolome of WT or indicated *P. inhibens* 2.10 mutants in response to pCA. The peak marked with a hashtag corresponds to roseobacticide A.

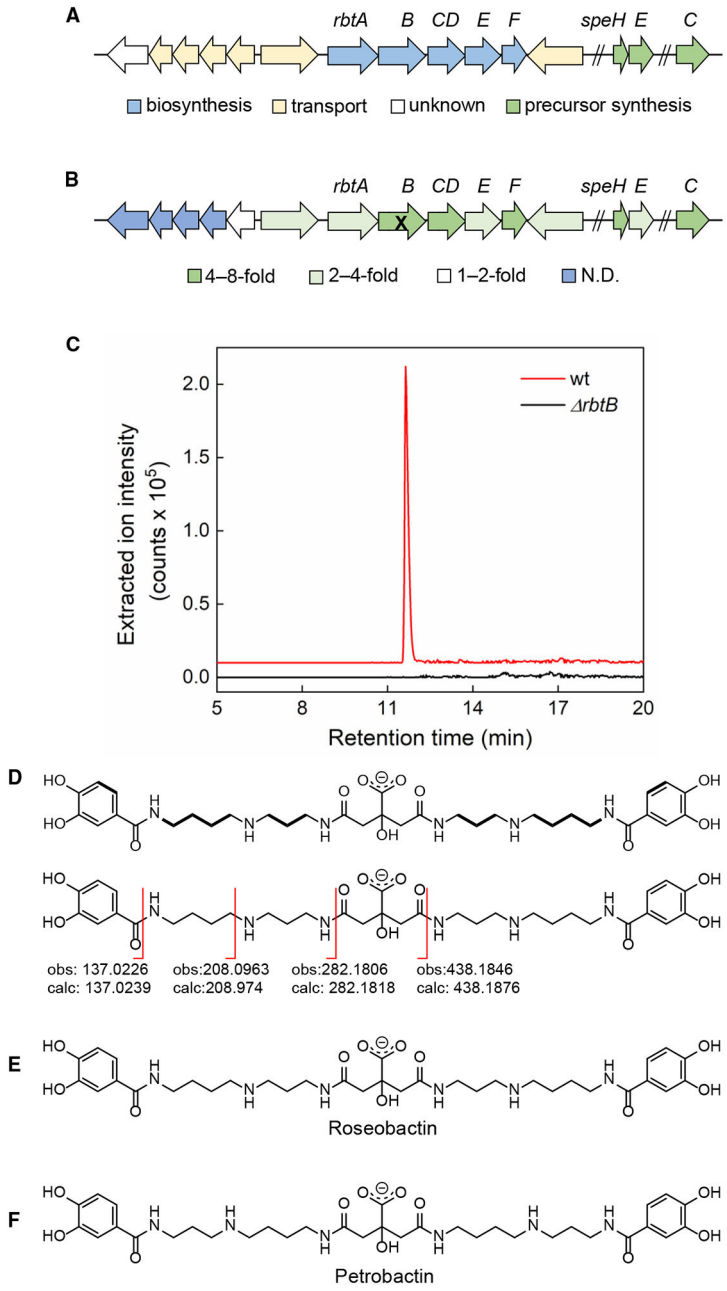

Figure 4. *P. inhibens* 2.10 upregulates the *rbt* cluster and produces roseobactin in response to pCA

(A) The *rbt* operon; genes are color coded as shown.

(B) Induction of the *rbt* cluster. Genes are color coded according to induction level in the presence of pCA. *RbtB*, deleted by mutagenesis in follow-up studies, is marked with an X.

(C) The *rbt* operon is responsible for production of a siderophore; deletion of *rbtB* abolishes siderophore synthesis, as shown by extracted ion chromatography (for m/z 719.3569).

(D) Structural elucidation of roseobactin by NMR spectroscopy (top, thick lines indicate COSY correlations) and by HR-MS/MS (bottom, observed fragments are shown).

(E) Structure of roseobactin, a new siderophore from *P. inhibens* 2.10.

(F) Structure of petrobactin.

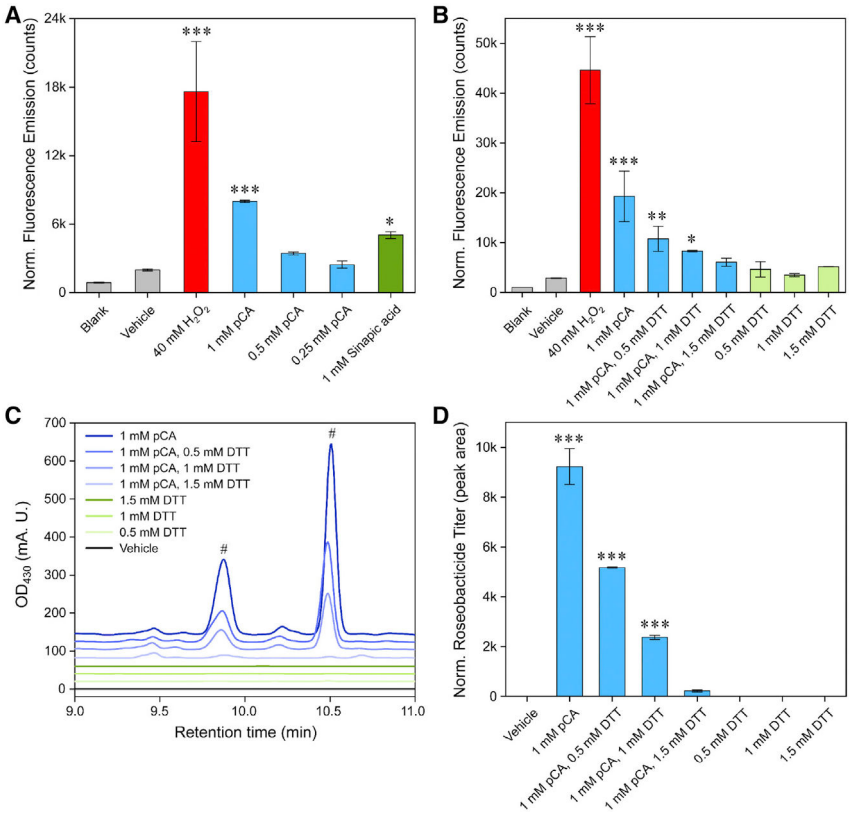

Figure 5. Roseobacticide production correlates with ROS levels

(A) Dose-dependent effect of pCA on ROS production, measured using an ROS-responsive fluorescent dye.

(B) Effect of DTT on pCA-mediated ROS production.

(C) Effect of DTT on pCA-mediated roseobacticide biosynthesis. Peaks marked with a hashtag correspond to roseobacticide A (left) and B (right).

(D) Quantification of roseobacticide biosynthesis from (C). In all panels, the averages of two independent replicates are shown; error bars represent standard error. “Vehicle” is the vehicle control, whereas “Blank” corresponds to a no-treatment condition. *$p < 0.05$, **$p < 0.005$, and ***$p < 0.001$, via an unpaired t test.

Table 1.

pCA treatment diminishes cellular energy supplies

Metabolite	Fold change
ATP	−2.6 ± 1.0
GTP	−3.1 ± 1.1
CTP	−2.9 ± 0.7
UTP	−2.5 ± 0.6
AMP	−1.5 ± 0.4
GMP	−2.9 ± 1.1
CMP	−1.9 ± 0.7
UMP	−2.1 ± 0.5
ADP	−2.1 ± 0.8
Glucose-1-phosphate	−4.8 ± 1.1
Glucose-6-phosphate	−4.8 ± 1.1
Phosphoenolpyruvate	−13.1 ± 7.9
Acetyl-CoA	−3.1 ± 1.8
NAD	−2.3 ± 0.4
NADP	−2.0 ± 0.6
NADPH	−2.0 ± 0.9

Shown are averaged, relative fold-change alterations in the metabolites indicated in response to pCA.

KEY RESOURCES TABLE

REAGENT or RESOURCE	SOURCE	IDENTIFIER
Bacterial and virus strains		
E. coli DH5α	NEB	Cat# C2987H
P. inhibens 2.10	Gift of Prof. Rebecca Case, University of Alberta	DSM 24588
Chemicals, peptides, and recombinant proteins		
Chloromethyl-H2DCFDA	ThermoFisher	Cat# C6827
Cyanine 3–cytidine-5′-triphosphate	Enzo Life Sciences	Cat# 42505
Cyanine 5–cytidine-5′-triphosphate	Enzo Life Sciences	Cat# 42506
Ethylenediaminetetraacetic acid	Sigma	Cat# E9884
Gentamycin Sulfate	Sigma	Cat# G1914
Hydrogen Peroxide	Fisher	Cat# H312
Kanamycin Sulfate	Sigma	Cat# 60615
Ammonium Bicarbonate	Fisher	Cat# A643
p-Chloro-phenylalanine	Fisher	Cat# AC157280050
p-Coumaric Acid	Sigma	Cat# C9008
Q5 DNA Polymerase	NEB	Cat# M0491
T4 Ligase	NEB	Cat# M020
T7 RNA polymerase	Agilent	Cat# 600123
Critical commercial assays		
Gene Expression Hybridization Kit	Agilent	Cat# 5188-5242
Quick Amp Labeling Kit	Agilent	Cat# 5190-0447
iScript cDNA Synthesis Kit	Bio-Rad	Cat# 1708890
Ambion DNA Free Kit	ThermoFisher	Cat# AM1906
iTaq Universal SYBR Green Supermix	Bio-Rad	Cat# 1725120
QIAquick Gel Extraction Kit	Qiagen	Cat# 28706X4
QIAquick PCR Purification Kit	Qiagen	Cat# 28104
RNEasy Mini Kit	Qiagen	Cat# 74104
Wizard gDNA Isolation Kit	Promega	Cat# A1120
Deposited data		
Complete microarray dataset	Mendeley Data	https://doi.org/10.17632/y8j4475s6v.1
Experimental models: organisms/strains		
P. inhibens 2.10 *ΔpaaC*	This Study	N/A
P. inhibens 2.10 *ΔpatB*	This Study	N/A
P. inhibens 2.10 *ΔrbtB*	This Study	N/A
P. inhibens 2.10 *Δtda*A	This Study	N/A
P. inhibens 2.10 *ΔtdaD*	This Study	N/A
Oligonucleotides		
Primers for molecular cloning, see Table S2		
Recombinant DNA		

REAGENT or RESOURCE	SOURCE	IDENTIFIER
pEX18Gm-pheS	Barrett et al., 2008	N/A
pRW01	Wang et al., 2016	N/A
Software and algorithms		
Feature Extract 12.0	Agilent	G4463AA
MAVEN 8.0	Melamud et al., 2010	http://maven.princeton.edu/index.php?show=download
RStudio 1.0	RStudio	https://www.rstudio.com/products/rstudio/download/#download
SAM (Statistical Analysis of Microarray) R package version 4.01	Tusher et al., 2001	https://github.com/MikeJSeo/SAM
OriginPro	OriginLab Corporation	https://www.originlab.com/origin
R code for running Statistical Analysis of Microarray (SAM)	Mendeley Data	https://doi.org/10.17632/y8j4475s6v.1
Other		
Agilent 1260 HPLC	Agilent	https://www.agilent.com/en/product/liquidchromatography
Agilent 6130 Quadrupole MS	Agilent	https://www.agilent.com/en/product/liquidchromatography-mass-spectrometry-lc-ms
Agilent 6540 qTOF MS	Agilent	https://www.agilent.com/en/product/liquidchromatography-mass-spectrometry-lc-ms
Bioanalyzer 2100	Agilent	Cat# G2939BA
CFX96 RT-PCR	Bio-Rad	Cat# 1855195
DNA Sequencing Micro Array Scanner	Agilent	Cat# G2506
H1MF Plate Reader	Biotek	N/A
Nanodrop ND-1000	ThermoFisher	N/A